This article is published as part of the *Dalton Transactions* themed issue entitled:

Synthetic Solid State Chemistry

Guest Editor Duncan Gregory
University of Glasgow, UK

Published in issue 26, 2010 of *Dalton Transactions*

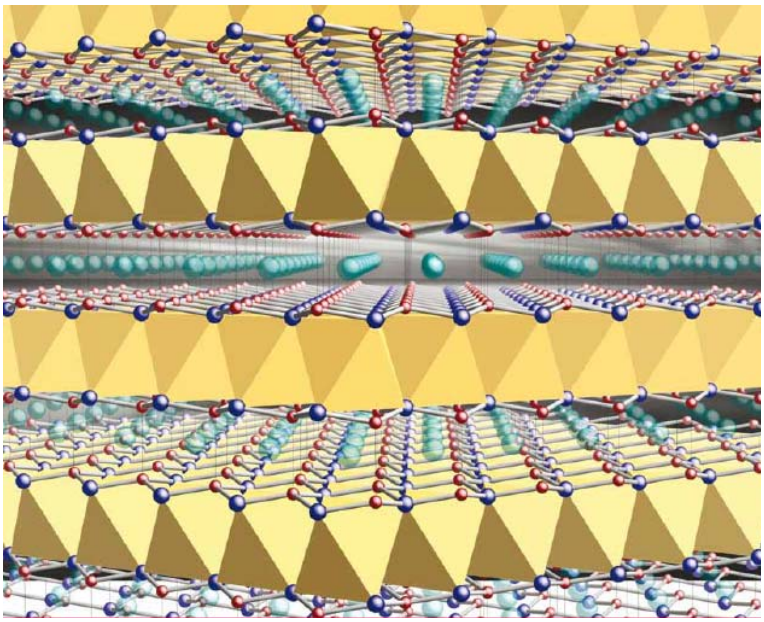

Image reproduced with the permission of Svilen Bobev

Articles in the issue include:

PERSPECTIVES:

COMMUNICATIONS:

Visit the *Dalton Transactions* website for more cutting-edge inorganic and solid-state research
www.rsc.org/dalton

Porous lanthanide oxides *via* a precursor method: Morphology control through competitive interaction of lanthanide cations with oxalate anions and amino acids†

Zhu-Rui Shen, Jin-Gui Wang, Ping-Chuan Sun, Da-Tong Ding and Tie-Hong Chen*

Received 5th August 2009, Accepted 9th November 2009
First published as an Advance Article on the web 11th January 2010
DOI: 10.1039/b916167h

Porous lanthanide oxides were fabricated by a precursor-thermolysis method. The precursors were synthesized by a hydrothermal reaction with lanthanide (La, Ce, Pr and Nd) salts, sodium oxalate and asparagine (or glutamine). Under hydrothermal conditions asparagine and glutamine exhibited greatly different complexation abilities with lanthanide cations. The competitive interactions of lanthanide cations with oxalate anions and asparagine (or glutamine) gave rise to the formation of precursors with different structures and morphologies. ESI-MS detection further confirmed the different complexation abilities of asparagine or glutamine with lanthanide cations at the molecular level. Variation of oxalate anion concentration or the pH value of the reaction solution could tune the morphology of the products. After calcination, porous lanthanide oxides were obtained with the morphologies of their corresponding precursors. Our work suggests that the complexation ability of organic molecules with metal cations could be a crucial factor for morphological control of the precursors. Moreover, considering the diversity of organic additives and metal salts, other metal oxides with complex composition and morphology could be fabricated *via* this organic molecule-modified precursor method.

Introduction

In recent years, the fabrication of porous metal oxides with pore size ranging from several to hundreds of nanometres has been extensively studied.[1–10] One common route to produce porosity is the template-based method, and soft templates (*e.g.* block copolymers, surfactants and emulsions)[11–15] and hard templates (*e.g.* mesoporous silica, carbon and polymer beads)[16–19] have been used. Another method named the 'metal salt precursor method' was developed as early as the 1980s, and it was successfully used to fabricate nanocrystalline metal oxides by simple thermal decomposition of metal salt precursors. The resultant oxides generally showed aggregation of fine crystallites, giving rise to mesopores (or macropores) as well as relatively large surface areas.[20–26] For example, Louër *et al.* prepared ZnO with a crystallite size of 10–20 nm by thermal decomposition of $Zn_3(OH)_4(NO_3)_2$.[20] Sankaranarayanan and co-workers fabricated ultrafine amorphous and crystalline $Dy_3Fe_5O_{12}$ using citrate $Dy_3Fe_5(cit)_{25}\cdot 36H_2O$ as the precursor.[21] Cu-Zn based manganites with specific surface area from *ca.* 30 to 50 $m^2\ g^{-1}$ were obtained after calcination of their carbonate precursors.[25] Besides, metal oxides nano-composites have also been prepared by a "single-source precursor" method in which the precursor of a molecular compound contains all the necessary elements of the final product.[27–29] Nanocrystalline lanthanide oxides have been fabricated by a cellulose-precursor method.[30] Inspired by these results, recently, our group has developed an amino-acid-modified oxalate precursor method to prepare hierarchically-structured mesoporous ceria.[31] Complex morphologies of the cerium oxalate precursors were fabricated under the control of amino acids as crystal-growth modifiers. After decomposition of the precursors by calcination, the morphologies

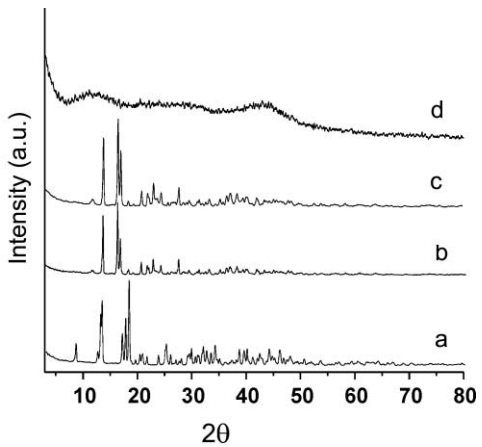

Fig. 1 XRD patterns of Ce-based products of (a) the initial products without hydrothermal treatment, (b) without additive, (c) with 6 mmol glutamine, (d) with 6 mmol asparagine, at reactant molar ratio (Ce^{3+}:oxalate) of 2 : 1.5 mmol after reaction at 160 °C for 48 h, respectively.

Institute of New Catalytic Materials Science, Key Laboratory of Energy-Material Chemistry (Tianjin) and Engineering Research Center of Energy Storage & Conversion (MOE), College of Chemistry, Nankai University, Tianjin 300071, PR China. E-mail: chenth@nankai.edu.cn; Fax: +86-22-23507975

† Electronic supplementary information (ESI) available: Optical photos, TEM and SEM images, N_2 sorption isotherms and XRD patterns. See DOI: 10.1039/b916167h

of the precursors remained and ceria nanoparticles were obtained to form mesoporous structures. Up to now, the metal salts precursor method has been widely used to prepare porous metal oxides assembled by nanoparticles.[32–40] For instance, mesoporous MnO_2 and NiO were fabricated by decomposition of their oxalate precursors[32,33] porous TiO_2 spheres were produced by *in situ* hydrolysis of titanium glycolate precursors,[34] and mesoporous MgO has been obtained through decomposition of magnesium carbonate hydrate.[35] Dimension-manipulated ceria nanostructures were obtained from a cerium octylate precursor.[36]

Very recently, we found asparagine had very strong complexation ability with lanthanide cations under hydrothermal conditions. Using asparagine as a ligand, lanthanide-based compound precursors with the morphologies of macroporous foams, microspheres and hollow spheres were fabricated successively, and porous lanthanide oxides with the morphology of their precursors were obtained after calcination.[41,42] These results inspired us to further study how the complexation ability of the amino acids influenced their morphology control effect on metal salt precursors. In this work we studied the competitive interaction of oxalate anions and amino acids (asparagine or glutamine) with lanthanide cations and lanthanide-based compound precursors with different structures and morphologies were obtained by tuning the competition effect of oxalate anions and amino acids.

Experimental

Glutamine (99%), asparagine (99%) and lanthanide salts (AR, including $La(NO_3)_3{\cdot}6H_2O$, $Ce(NO_3)_3{\cdot}6H_2O$, $CeCl_3{\cdot}7H_2O$, $Pr(NO_3)_3{\cdot}6H_2O$, $Nd(NO_3)_3{\cdot}6H_2O$) were commercial products and used as-received.

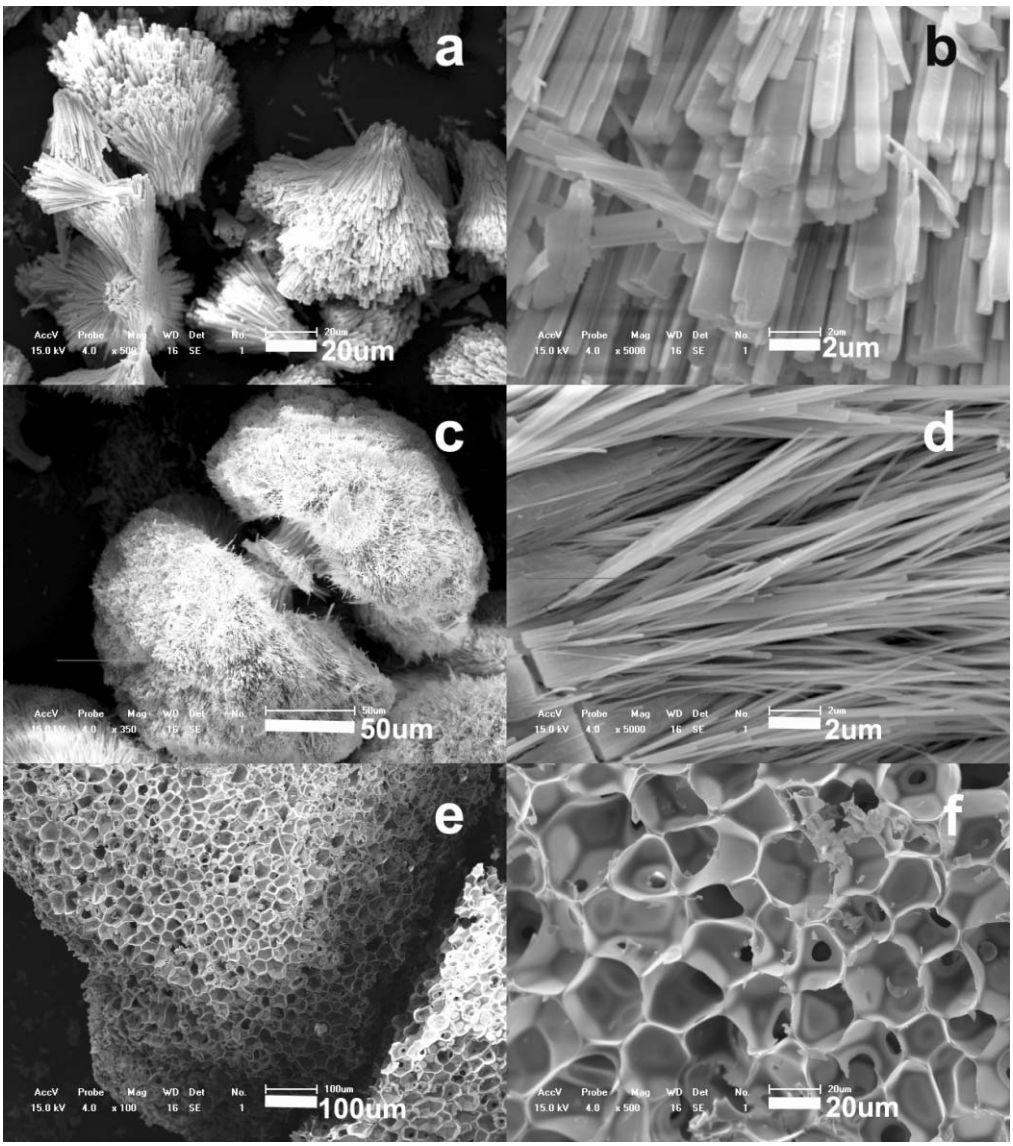

Fig. 2 SEM images of (a, b) cerium oxalate obtained at a reactant molar ratio (Ce^{3+}:oxalate) of 2:1.5, (c, d) cerium oxlate obtained at a reactant molar ratio (glutamine:Ce^{3+}:oxalate) of 6:2:1.5, (e, f) Ce-organic complexation compound foam obtained at reactant molar ratio (asparagine:Ce^{3+}:oxalate) of 6:2:1.5, after hydrothermal reaction at 160 °C for 48 h.

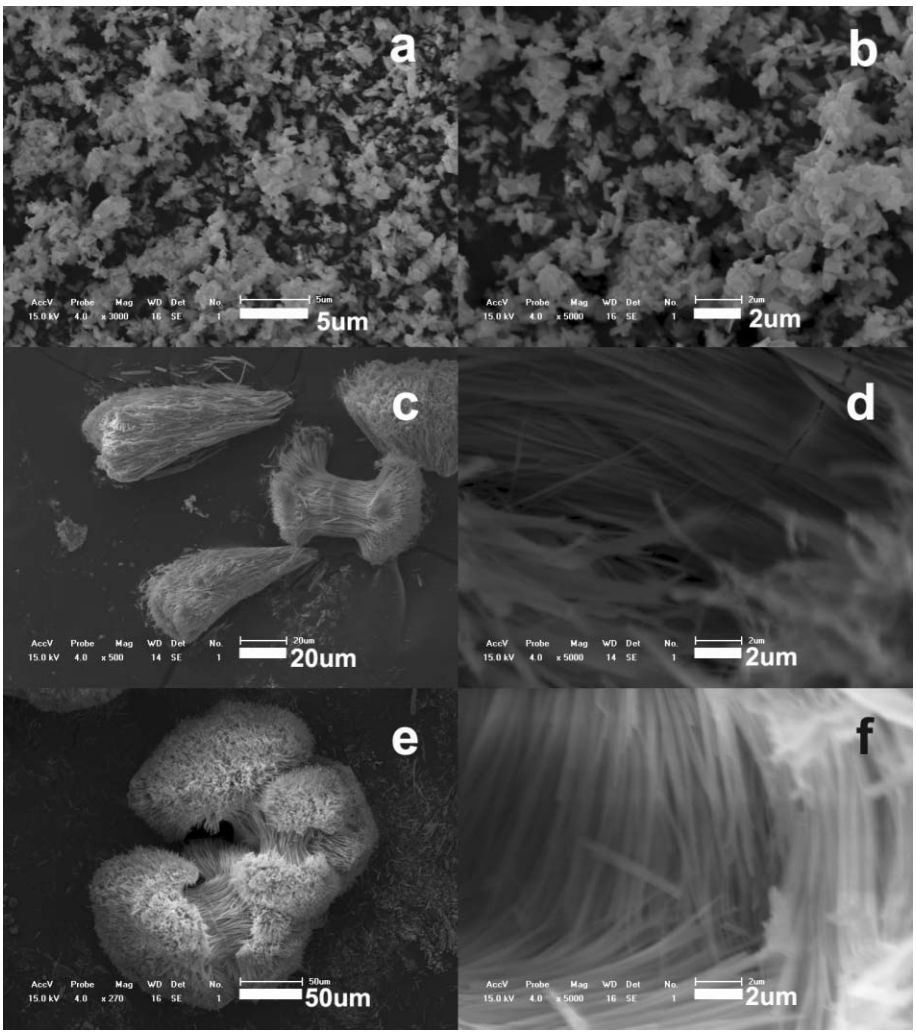

Fig. 3 SEM images of cerium oxalate products obtained at a reactant molar ratio (glutamine:Ce^{3+}:oxalate) of 6:2:1.5 after reaction at 160 °C for (a, b) 0 h, (c, d) 5 h, (e, f) 12 h. The quantity of glutamine was 6 mmol in the synthesis.

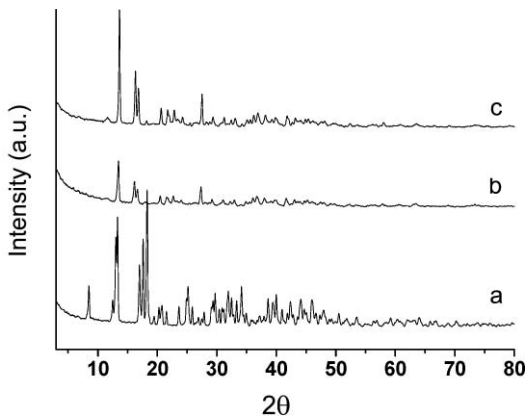

Fig. 4 XRD patterns of Ce-based products obtained at reactant molar ratio (glutamine:Ce^{3+}:oxalate) of 6:2:1.5) after reaction at 160 °C for (a) 0 h, (b) 5 h, (c) 12 h. The quantity of glutamine was 6 mmol in the synthesis.

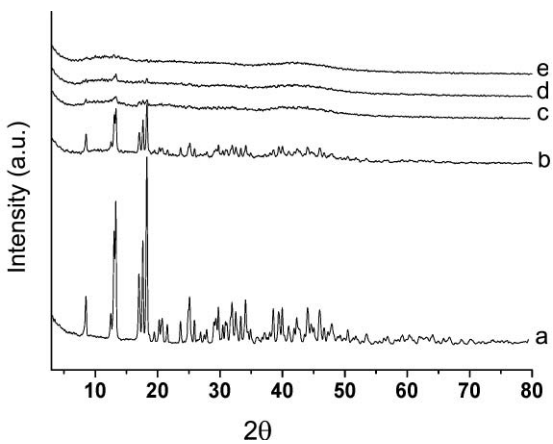

Fig. 5 XRD patterns of products obtained at reactant molar ratio (asparagine:Ce^{3+}:oxalate) of 6:2:1.5 after reaction at 160 °C for (a) 0 h, (b) 1 h, (c) 2 h, (d) 6 h, (e) 24 h. The quantity of asparagine was 6 mmol in the synthesis.

For electrospray ionization mass spectrometry (ESI-MS), 6 mmol asparagine was dissolved in 24 mL deionized water at 45 °C, and then 0.5 mmol $Nd(NO_3)_3{\cdot}6H_2O$ was added under stirring. After 10 min, the solution was transferred to a 30 mL Teflon-lined autoclave, sealed and hydrothermally treated at 120 °C for a certain time. After hydrothermal treatment the solutions were diluted with methanol and subjected to ESI-MS analysis.

For the synthesis of lanthanide oxalate nanofibers and their oxides, 6 mmol glutamine was dissolved in 12 mL deionized water at 45 °C and then 2 mmol lanthanide salt ($La(NO_3)_3{\cdot}6H_2O$, $CeCl_3{\cdot}7H_2O$, *etc.*) was added under stirring. Next the solution was mixed with 12 mL $Na_2C_2O_4$ solution (1.5 mmol) and immediately a suspension was obtained. After being stirred for 30 min the suspension was transferred to a 30 mL Teflon-lined autoclave, sealed and hydrothermally treated at 160 °C for 48 h. The product powders were collected and were washed with deionized water and ethanol thoroughly. Ceria nanofibers were obtained after calcination of the precursors at 360 °C for 1 h, while other lanthanide oxide nanofibers were obtained after calcination of the precursors at 720 °C for 4 or 5 h.

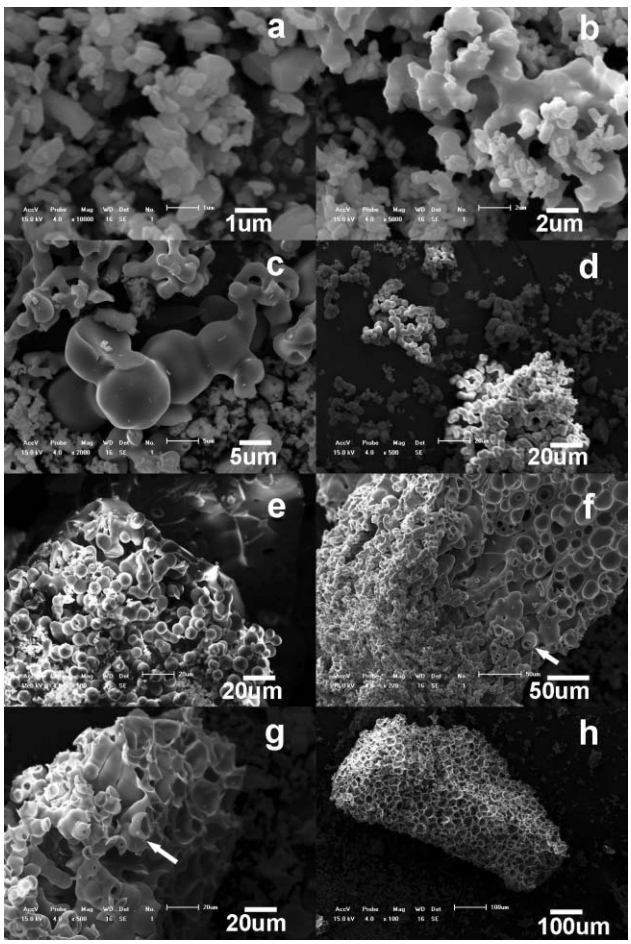

Fig. 6 SEM images of Ce-based products obtained at reactant molar ratio (asparagine:Ce^{3+}:oxalate) of 6:2:1.5 after reaction at 160 °C for (a) 0 h, (b, c) 1 h, (d, e) 2 h, (f) 6 h, (g) 12 h, (h) 24 h. The arrows in (f, g) indicate some hollow spheres. The quantity of asparagine was 6 mmol in the synthesis.

Table 1 The fractional ions detected by ESI-MS after different times of the Nd^{3+}–asparagine and Nd^{3+}–glutamine reaction systems at 120 °C

Reaction time	Nd^{3+}–asparagine reaction system Fractional ions detected	Nd^{3+}–glutamine reaction system Fractional ions detected
0	$[Nd(C_4H_7O_3N_2)_2]^+$ (*m*/*z* 400.99) $[Nd(C_4H_7O_3N_2)_3+H]^+$(*m*/*z* 533.05)	$[Nd(C_5H_9O_3N_2)_2]^+$ (*m*/*z* 432.02) $[Nd(C_5H_9O_3N_2)_3+H]^+$ (*m*/*z* 578.10)
30 min	$[Nd_3(C_4H_7O_3N_2)_7]^{2+}$ (*m*/*z* 674.52) $[Nd_4(C_4H_7O_3N_2)_9+H]^{2+}$ (*m*/*z* 878.04) $[Nd_5(C_4H_7O_3N_2)_{12}]^{3+}$ (*m*/*z* 764.72)	$[Nd_2(C_5H_9O_3N_2)_5]^+$ (*m*/*z* 1013.12) $[Nd_3(C_5H_9O_3N_2)_7]^{2+}$ (*m*/*z* 723.59) —
60 min	$[Nd_3(C_4H_7O_3N_2)_6(C_4H_6O_4N)]^{2+}$ (*m*/*z* 675.01) $[Nd_2(C_4H_7O_3N_2)_5]^+$ (*m*/*z* 472.02)	$[Nd(C_5H_9O_3N_2)_4+2H]^+$ (*m*/*z* 726.16) $[Nd(C_5H_9O_3N_2)_6+5H]^{2+}$ (*m*/*z* 509.66) $[Nd_2(C_5H_9O_3N_2)_7+3H]^{2+}$ (*m*/*z* 653.13)
90 min	No fractional ions detected (solid particles appeared) — —	$[Nd(C_5H_9O_3N_2)_4+2H]^+$ (*m*/*z* 726.16) $[Nd(C_5H_9O_3N_2)_6+5H]^{2+}$ (*m*/*z* 509.66) $[Nd_2(C_5H_9O_3N_2)_7+3H]^{2+}$ (*m*/*z* 653.13)
120 h	No fractional ions detected Monolithic foam product obtained, light-brown solution	No fractional ions detected No solid product obtained, dark-brown solution

For the synthesis of 3D macroporous lanthanide compound foams and their oxides, the procedure was same as the above paragraph, except that 6 mmol asparagine was used instead of glutamine. The quantity of $Na_2C_2O_4$ was tuned as 0, 1.5 and 3 mmol, respectively. Dilute NaOH or HCl solution was used to tune the pH value of the solution if necessary. As-synthesized samples were usually collected as monoliths and were washed with deionized water and ethanol thoroughly. Ceria foams were obtained after calcination of precursors at 360 °C for 1 h, while other lanthanide oxide foams were obtained after calcination of precursors at 720 °C for 2 or 5 h.

XRD patterns were recorded with a Rigaku D/max-2500 diffractometer. SEM and TEM images were measured on Shimadzu SS-550 and Philips Tecnai F20 instruments, respectively. N_2 adsorption isotherms were measured on a BELSORP mini II analyzer. Elemental analysis data was obtained with an Elementar Vario-EL instrument. Electrospray ionization mass spectra were obtained on an IonSpec 7.0 T FTICR-MS (ESI source) instrument.

Results and discussion

Cerium oxalate based precursors in the presence of glutamine and asparagine, respectively

In the synthesis process, upon the addition of sodium oxalate to the solution of Ce^{3+}, a white precipitate was formed immediately, which was identified as $Ce_2(C_2O_4)_3{\cdot}10H_2O$ by its XRD pattern (Fig. 1a). However, during the subsequent hydrothermal treatment, different products were obtained depending on the presence

of asparagine or glutamine, respectively. Without the addition of amino acid, the XRD pattern (Fig. 1b) shows the product was a crystalline phase. To our knowledge it could not be ascribed to any known structure, and this product was just denoted as "oxalate A", which should be a more stable cerium oxalate phase and its growth was accompanied with the dissolution of $Ce_2(C_2O_4)_3{\cdot}10H_2O$. The morphology of the product was dumbbell-like bundles of densely packed microrods (Fig. 2a and b). When glutamine was added, the crystal structure was also determined to be "oxalate A" (Fig. 1c) and the morphology of the product was dumbbell-like particles assembled as nanorods (Fig. 2c and d). The products synthesized with or without glutamine exhibited the same crystal structure, which implies that glutamine was not involved in the crystal structure of "oxalate A", and it acted only as the crystal-growth modifier,[43] which could control the nucleation and epitaxial growth of the cerium oxalate crystals.

The time dependent syntheses of Ce-precursors were performed under 160 °C in the presence of glutamine. The initial precipitates produced without hydrothermal treatment were microcrystals with a size of ~1 μm (Fig. 3a and b), and the XRD patterns (Fig. 4a) showed that they were pure $Ce_2(C_2O_4)_3{\cdot}10H_2O$. After 5 h of reaction, the dumbbell-like nanorod aggregation appeared (Fig. 3c and d), and its XRD pattern (Fig. 4b) indicated the structure of "oxalate A". With the reaction proceeding to 12 h, the assembly of nanorods became the majority of the final products (Fig. 3e and f), meanwhile its corresponding XRD pattern showed they were pure "oxalate A" (Fig. 4c). Although glutamine is able to form complexes with lanthanide cations, the electrostatic interaction between lanthanide cations and oxalate anions is obviously stronger, and after the hydrothermal treatment only lanthanide oxalate crystals were obtained.

However, in the presence of asparagine, the final product was a white monolith (Fig. S1 of the ESI†) floating in the reaction solution. The XRD pattern of the product was featureless (Fig. 1d), indicating its amorphous nature. As shown in Fig. 2e and f, the monolith displayed a 3D macroporous foam-like morphology, with the cellular size ranging from 20 to 50 μm. Elemental analysis showed that it had a high organic species content (5.1 wt% of nitrogen), and the foam-like monolith was a kind of cerium compound. During the reaction process, after hydrothermal treatment for 1 h, the initial microcrystals of $Ce_2(C_2O_4)_3{\cdot}10H_2O$ (Fig. 5a) began to merge together and some microspheres formed (Fig. 6a, b and c). The corresponding XRD pattern displayed lower crystalline peaks which were assigned to $Ce_2(C_2O_4)_3{\cdot}10H_2O$ (Fig. 5b). This indicated that the microspheres formed at the expense of $Ce_2(C_2O_4)_3{\cdot}10H_2O$ crystals, and the asparagine in the solution competed with oxalate anions to bind with lanthanide cations to form the amorphous compound. After 2 h of reaction, the monolithic blocks from the aggregation of microspheres became the main product (Fig. 6d and e), meanwhile several weak crystalline peaks corresponding to residual $Ce_2(C_2O_4)_3{\cdot}10H_2O$ crystals could be found in the XRD pattern (Fig. 5c). After 6 h and 12 h, many holes began to emerge on the block and some spheres not totally fused into the block became hollow simultaneously (Fig. 6f and g). This implies that the solid spheres totally merged into the block would undergo the same

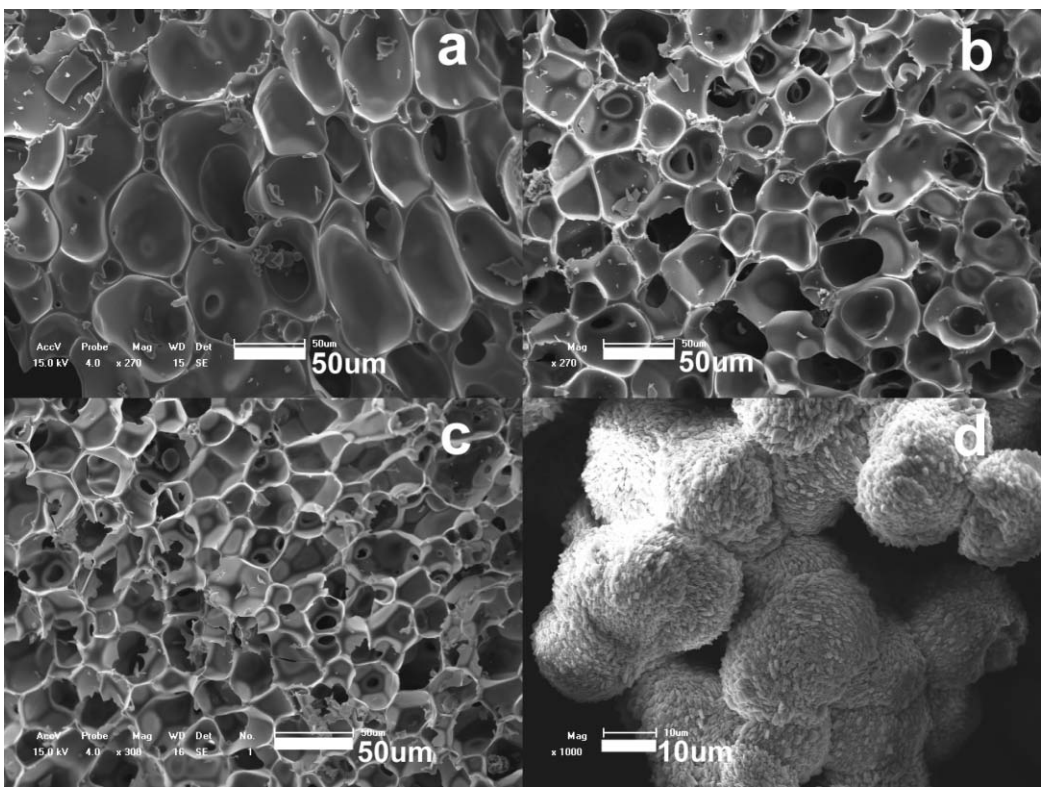

Fig. 7 SEM images of Ce-based products obtained at different reactant molar ratios (asparagine:Ce^{3+}:oxalate) of (a) 6:2:0, (b) 6:2:075, (c) 6:2:1.5, (d) 6:2:3, after reaction at 160 °C for 48 h.

hollowing process, gradually developing into the 3D macroporous foam-like structure. When the reaction proceeded to 24 h, the 3D macroporous foam was obtained (Fig. 6h) and its XRD pattern finally became featureless (Fig. 5e). From the above results, it is found that the hollowing process was similar to the previously reported one based on an Ostwald ripening mechanism.[41] This is to say that during the hydrothermal reaction, asparagine grabbed the lanthanide cations from the starting $Ce_2(C_2O_4)_3{\cdot}10H_2O$ *via* a complexation interaction to form the compound foam.

Compared with the case of glutamine addition, it is proposed that under hydrothermal conditions the complexation interaction between asparagine and lanthanide cations is stronger than the electrostatic interaction between oxalate anions and lanthanide cations, and the latter is stronger than that between glutamine and lanthanide cations, as discussed above. Although glutamine and asparagine differ only by a CH_2 group (Scheme S1 of the ESI†), they exhibited different morphology control processes due to their difference in complexation ability with lanthanide cations. The competitive complexation of amino acids and oxalate anions occurred from the initial stage of the hydrothermal reaction and determined the composition and morphology of the precursors during the succeeding reaction stages, as discussed later.

Complexes formation by asparagine/glutamine and lanthanide cations as monitored by ESI-MS

From the time-dependent experiments described above, it was found that asparagine and glutamine induced different morphologies for cerium oxalate precursors. Moreover, similar phenomena were also found when other lanthanide cations (*e.g.* La^{3+}, Pr^{3+}, Nd^{3+}) were used instead of cerium ions, and we ascribed these phenomena to different complexation ability of asparagine and glutamine with lanthanide cations under hydrothermal conditions. Asparagine binds to lanthanide cations more strongly than glutamine under these conditions, and was able to grab cations from the crystalline lanthanide oxalates and finally form an amorphous compound. The cation–ligand complexes and the monomer of the coordination polymer could be effectively examined by ESI-MS.[44-48] Our testing system was simple, and contained only asparagine (or glutamine), Nd^{3+} and H_2O (please note that no

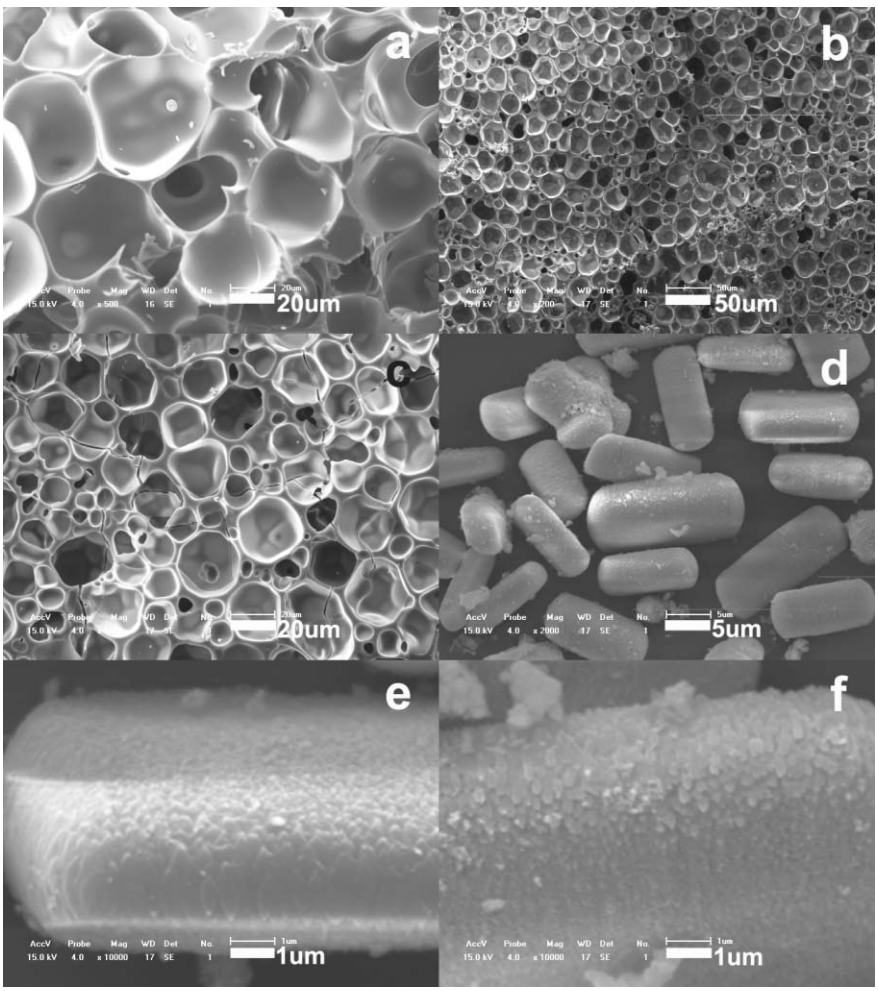

Fig. 8 SEM images of Ce-based precursors obtained at reactant molar ratios (asparagine:Ce^{3+}:oxalate) of 6:2:1.5 and with the pH value of 3.0 (a), 7.0 (b, c) and 9.0 (d, e, f) after reaction at 160 °C for 48 h.

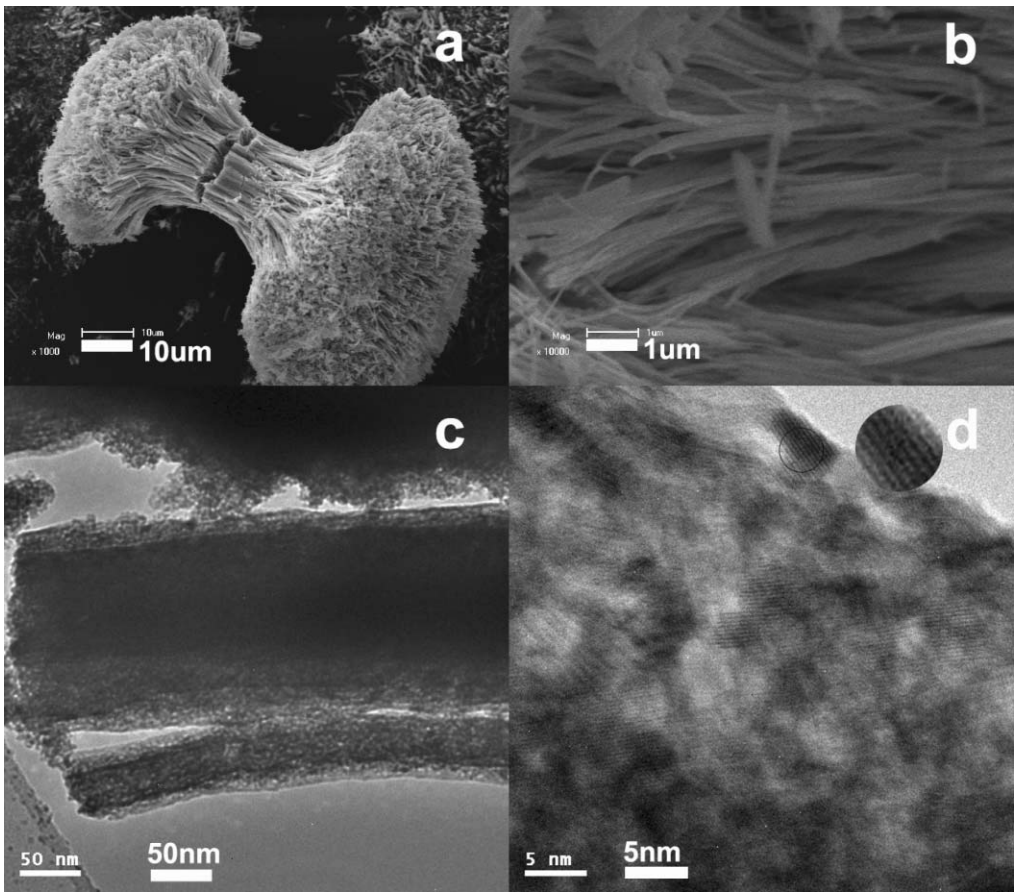

Fig. 9 SEM images of (a, b) ceria nanofibers obtained at reactant molar ratio (glutamine:Ce^{3+}:oxalate) of = 6:2:1.5 after reaction at 160 °C for 48 h, and was followed by calcination at 360 °C for 1 h. The glutamine was 6 mmol in the synthesis. (c, d) TEM images, the inset in (d) displays the interplanar spacing of the (111) facet.

sodium oxalate was added). Here we chose Nd^{3+} as the model lanthanide cation because of its specific isotope distribution in ESI-MS detection. A lower temperature of 120 °C was selected for a slower reaction process. The initial solution before hydrothermal treatment and the solution after hydrothermal reaction for 30, 60 and 90 min, respectively, were measured by ESI-MS and the results are listed in Table 1.

It was found that in the initial solution asparagine ($[H^+(C_4H_7O_3N_2)^-]$) coordinated with Nd^{3+}, and ESI-MS peaks at m/z 400.99 (with its isotope peaks) and 533.05 (with its isotope peaks) could be assigned to the mononuclear complexes $[Nd(C_4H_7O_3N_2)_2]^+$ and $[Nd(C_4H_7O_3N_2)_3 + H^+]$. After hydrothermal treatment for 30 min, the initial mononuclear complexes began to connect and multi-nuclear complexes were formed, such as $[Nd_3(C_4H_7O_3N_2)_7]^{2+}$ (m/z 674.52 with its isotope peaks), $[Nd_4(C_4H_7O_3N_2)_9]^{3+}$ (m/z 878.04 with its isotope peaks) and $[Nd_5(C_4H_7O_3N_2)_{12}]^{3+}$ (m/z 764.72 with its isotope peaks). When asparagine reacted with lanthanide cations, the multi-nuclear complexes with four or five metal ions might be crucial for the formation of larger frameworks of compound precursors. When the hydrothermal reaction proceeded for 60 min, the four- and five-nuclear complexes were absent while the fractional ions $[Nd_2(C_4H_7O_3N_2)_5]^+$ (m/z 472.02 with its isotope peaks) and $[Nd_3(C_4H_7O_3N_2)_6(C_4H_6O_4N)]^{2+}$ (m/z 675.01 with its isotope peaks) were detected. This implied that multi-nuclear complexes were further connected and the framework of compounds began to emerge. Notably, parts of the asparagine ligands were transformed into aspartic acids, providing direct evidence for the structural transformation of asparagine to aspartic acid ($C_4H_7O_4N$), which was proposed by EA, XPS and NMR analyses in our previous work.[41] Furthermore, after 90 min of hydrothermal treatment, no fractional ions containing asparagine or aspartic acid ligands could be detected, and it is quite reasonable to speculate that much larger molecular complexes beyond ESI-MS detection were obtained. Finally after hydrothermal treatment at 120 °C for 120 h, a solid Nd–organic foam with aligned macropores was produced.[41] At this stage, for the remaining solution, there were no fractional ions detected by ESI-MS. This could be ascribed to the formation of compound monoliths which consumed most of the molecular complexes in the solution. Although there were molecular complexes left in the solution, their thermal stability was much weaker than that of the rigid coordination framework. So after hydrothermal treatment as long as 120 h, those complexes in solution would be decomposed (the reaction solution became light brown) and thus no fractional ions could be detected by ESI-MS.

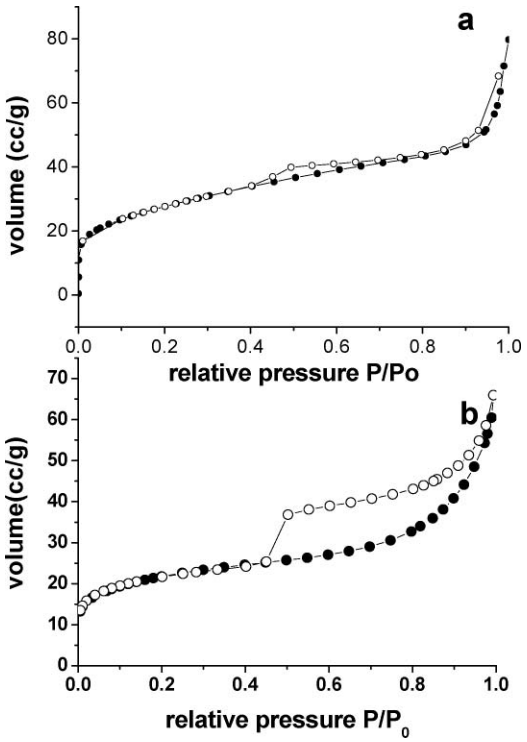

Fig. 10 Nitrogen adsorption–desorption isotherms of (a) CeO_2 nanofibers and (b) CeO_2 foam.

In the case of glutamine ($[H^+(C_5H_9O_3N_2)^-]$), in the initial solution the mononuclear complexes $[Nd(C_5H_9O_3N_2)_2]^+$ (*m*/*z* 432.02 with its isotope peaks) and $[Nd(C_5H_9O_3N_2)_3 + H^+]$ (*m*/*z* 578.10 with its isotope peaks) were found, which indicated that glutamine could also bind to lanthanide cations by complexation interaction. After hydrothermal reaction for 30 min, the mononuclear complex also began to become connected, however, the multi-nuclear complexes only contained two or three metal ions: $[Nd_2(C_5H_9O_3N_2)_5]^+$ (*m*/*z* 1013.12 with its isotope peaks) and $[Nd_3(C_5H_9O_3N_2)_7]^{2+}$ (*m*/*z* 723.59 with its isotope peaks), and this could be ascribed to larger spatial resistance when lanthanide cations coordinated with glutamine, whose molecular size is larger than that of asparagine. Moreover, it is speculated that the complexes formed based on these multi-nuclear complexes might not be large enough to form the amorphous compound particles. After 60 min of hydrothermal treatment, fractional ions $[Nd(C_5H_9O_3N_2)_4 + 2H]^+$ (*m*/*z* 726.16 with its isotope peaks), $[Nd(C_5H_9O_3N_2)_6 + 5H]^{2+}$ (*m*/*z* 509.66 with its isotope peaks) and $[Nd_2(C_5H_9O_3N_2)_7 + 3H]^{2+}$ (*m*/*z* 653.13 with its isotope peaks) were found in the reaction solution. However, when the hydrothermal treatment proceeded to 90 min, the fractional ions detected remained the same as the results after hydrothermal treatment of 60 min, indicating that the molecular complexes containing only two or three metal ions could not further connect to form the larger compound framework. Finally after hydrothermal treatment at 120 °C for 120 h, no solid products could be obtained when using glutamine as ligand, and

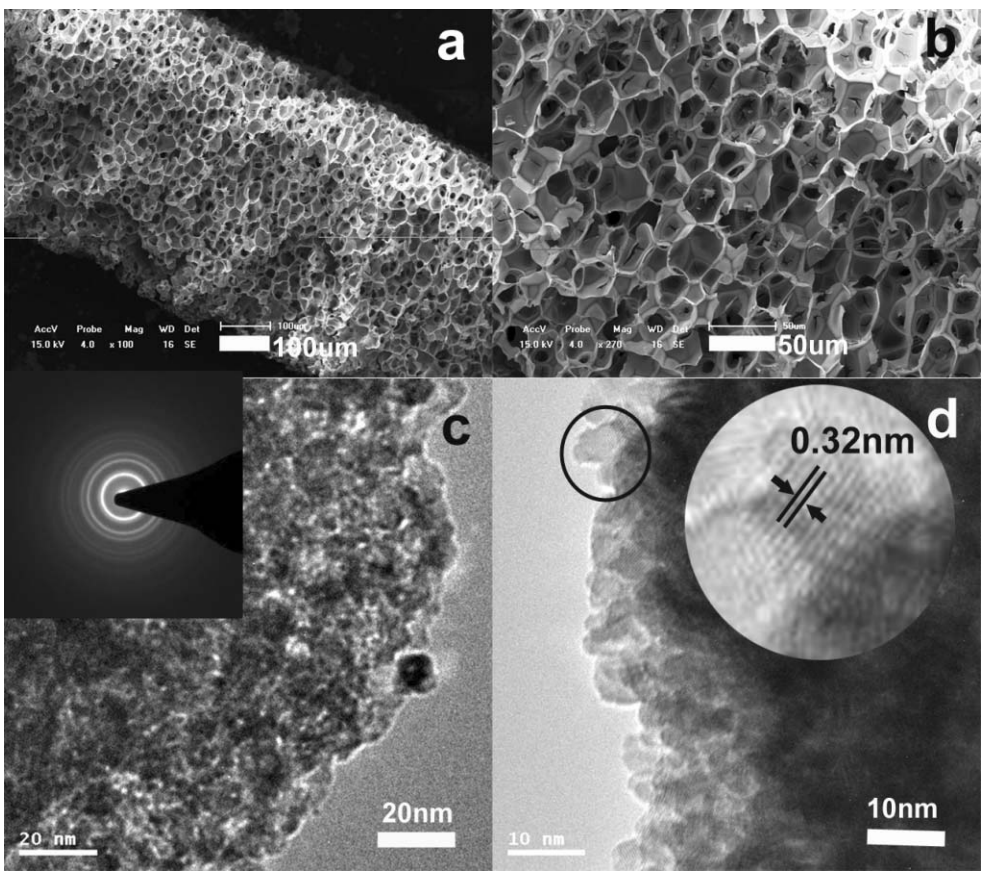

Fig. 11 SEM images of (a, b) CeO_2 foam obtained at reactant molar ratio (asparagine:Ce^{3+}:oxalate = 6:2:1.5) after reaction at 160 °C for 48 h, and was followed by calcination at 360 °C for 1 h. (c, d) TEM images of CeO_2 foam, the inset picture in (c) is its corresponding SAED pattern, and the inset picture in (d) displaying the interplanar spacing of the (111) facet.

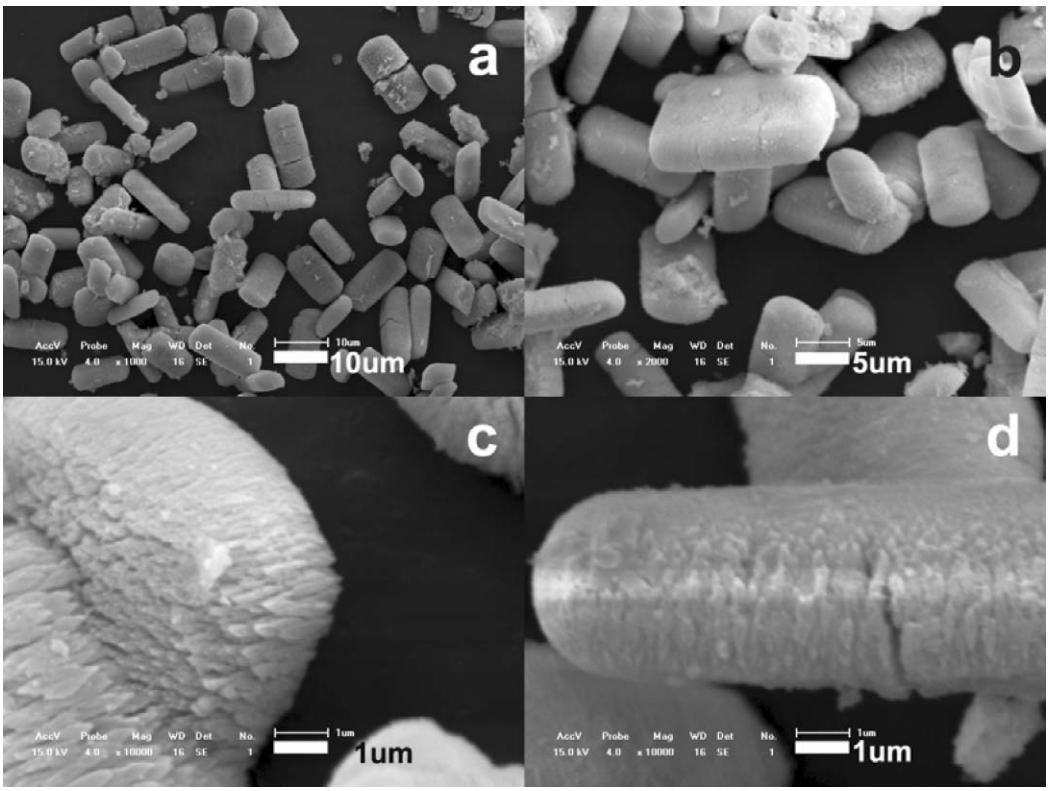

Fig. 12 SEM images of bread-like ceria particles assembled as nanoflakes obtained by the thermolysis of the corresponding cerium-based precursors.

the solution turned to brown due to the decomposition of the glutamine which could not form solid compound particles with lanthanide cations. As a result, we could not find any amino-acid-containing fractional ions from the solution after hydrothermal treatment at 120 °C for 120 h.

Based on the results of ESI-MS, we could conclude that: i) for asparagine, the final product originated from mononuclear complexes that grew to form some crucial multi-nuclear complexes with more than four metal ions, and further connect to form the solid compound; ii) for glutamine, it could also bind with lanthanide cations to form mononuclear complexes initially, however, only transient multi-nuclear complexes with fewer than three metal ions could be formed because of larger spatial resistance, and these multi-nuclear complexes could not connect together to form any solid product.

Morphology control of lanthanide-based precursors in the presence of asparagine by tuning the concentration of oxalate anions and pH values

As discussed above, the cerium macroporous precursor was proven to be an amorphous compound and there were mutual complexation interactions between Ce^{3+}, oxalate anions and asparagine. Varying the concentration of any species would change the complexation interactions between them, and then would influence the morphology of the product. So we performed synthesis with different concentrations of the oxalates. SEM observation showed that without the addition of oxalate ions, a macroporous foam with low porosity and thick walls was produced (Fig. 7a). After addition of a certain quantity of oxalate ions, lanthanide 3D macroporous foams with higher porosity were obtained (Fig. 7b and c). However, when the concentration of the oxalate ions was increased further, only crystalline microparticles were obtained (Fig. 7d, for the XRD pattern see Fig. S2 of the ESI†). EA analysis showed that the N content in those crystalline microparticles is 1.48 wt%, which is nearly one third of that detected in the 3D macroporous foam produced with the addition of 1.5 mmol oxalates (5.1 wt%). This means that the oxalate anions could still competitively bind with the lanthanide cation depending on its concentration.

On the basis of the results mentioned above, it is verified again that there existed a complexation–dissociation balance between oxalate anions, lanthanide cations and asparagine, and this balance determined the growth process of the compound. When the concentration of oxalates was changed, a new balance would be formed and thus a new growth process would produce a final product with a different macroporosity.

The ionization balance of asparagine determined the concentration of deprotonated asparagine in solution,[49] and it could be altered easily by tuning the pH value of the reaction solution. Considering complexes were formed by deprotonated asparagine and lanthanide cations, according to ESI-MS, the complexation–dissociation balance between oxalate anions, lanthanide cations and asparagine could also be changed by altering the pH value of the reaction solution, thus the morphology of cerium precursors were tuned simultaneously. When the pH value of the reaction solution was tuned to 3.0, macroporous foams (Fig. 8a) with lower porosity and thick walls were produced. When the pH value reached 7.0, it is interesting that the foams had two kinds of pore size distribution of 20–40 μm and 4–10 μm (Fig. 8b and

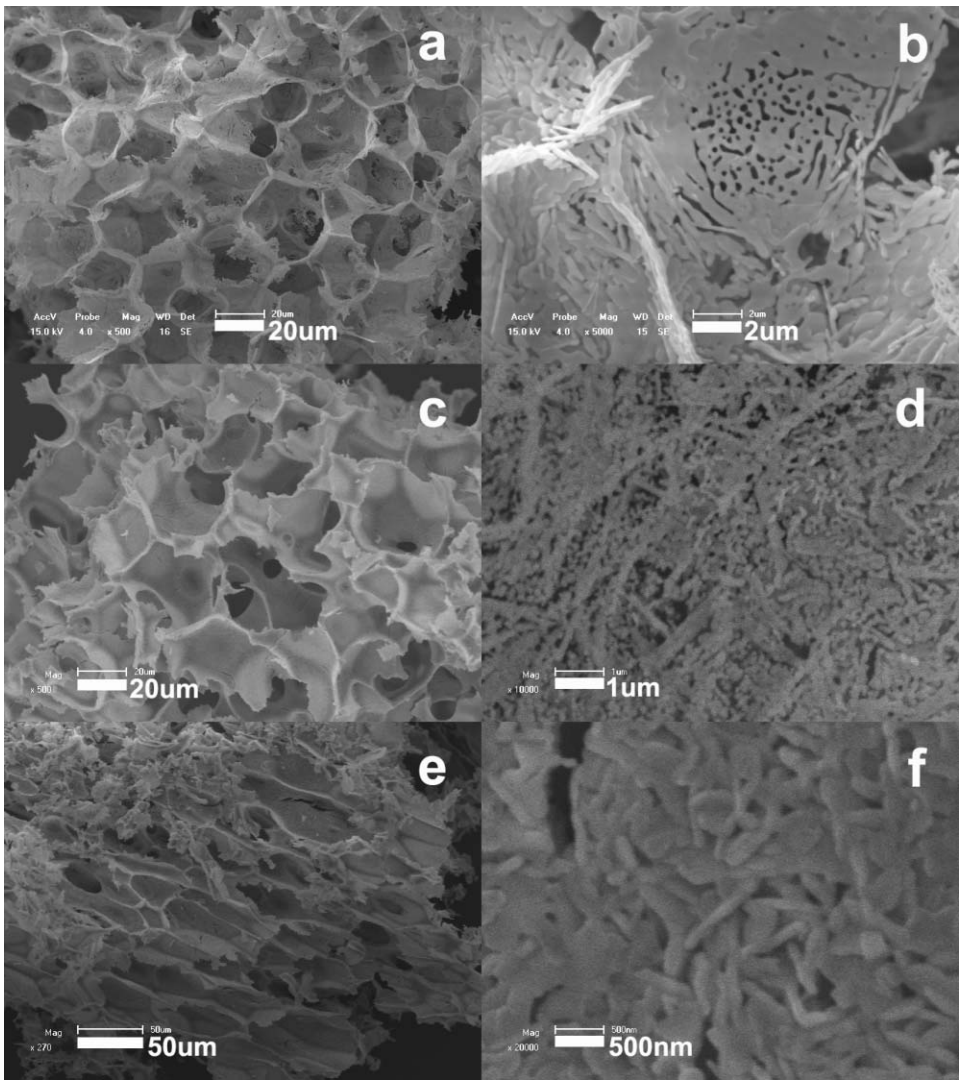

Fig. 13 SEM images of porous–macroporous materials of (a, b) La_2O_3, (c, d) Pr_6O_{11}, (e, f) Nd_2O_3.

c). However, when the pH value was tuned to 9.0 the macroporous foam disappeared and crystalline bread-like particles assembled as rhombic nanoflakes were obtained (Fig. 8d–f). The XRD patterns showed it had the same crystal phase (Fig. S3†) to the microparticles produced under high oxalate concentrations, which was noted as "oxalate B".

Porous lanthanide oxides obtained by thermolysis of lanthanide-based precursors

Ceria materials were produced by the thermolysis of cerium-based precursors. After calcination in air, the morphology of the precursors obtained under control of glutamine remained stable (Fig. 9a) and the XRD pattern showed it was pure ceria (Fig. S4a). From the SEM image (Fig. 9b), it is observed that the dumbbell-like particles were composed of oriented nanofibers (200–400 nm in diameter). The TEM image showed the aggregation of ceria nanoparticles (Fig. 9d) with a BET surface area of 99 $m^2\ g^{-1}$ as well as a pore volume of 0.072 $cm^3\ g^{-1}$ (Fig. 10a). For the Ce-coordination compound monolithic foam as precursor, after calcination in air, the monolithic shape remained with a yellowish color as well as a foam-like morphology (Fig. 11a and b). Ceria nanoparticles were generated, as revealed by the TEM images (Fig. 11c and d) and the relatively broad peaks in the XRD pattern (Fig. S4b) of the calcined foam. The 0.32 nm spacing between two adjacent lattice planes corresponds to the separation of the (111) lattice planes of the ceria. The selected-area electron diffraction (SAED) pattern (inset of Fig. 11c) clearly displays diffraction rings, indicating the polycrystalline nature of the foam wall. The BET surface area of the CeO_2 foam was 78 $m^2\ g^{-1}$, with a pore volume of 0.084 $cm^3\ g^{-1}$ (Fig. 10b). After calcination, bread-like ceria particles assembled as nanoflakes were produced (Fig. 12) with a BET surface area of 35 $m^2\ g^{-1}$ (Fig. S5).

This amino-acid-modified precursor method could be easily expanded to prepare other lanthanide oxides, such as La_2O_3, Pr_6O_{11} and Nd_2O_3. When using glutamine as the additive, after decomposition of the corresponding precursors, bi-pyramidal particles of La_2O_3 nanofibers (Fig. S6a and b), dumb-bell assemblies of Pr_6O_{11} nanofibers (Fig. S6c and d) and dispersed Nd_2O_3 nanofibers were prepared (Fig. S6e and f), respectively.

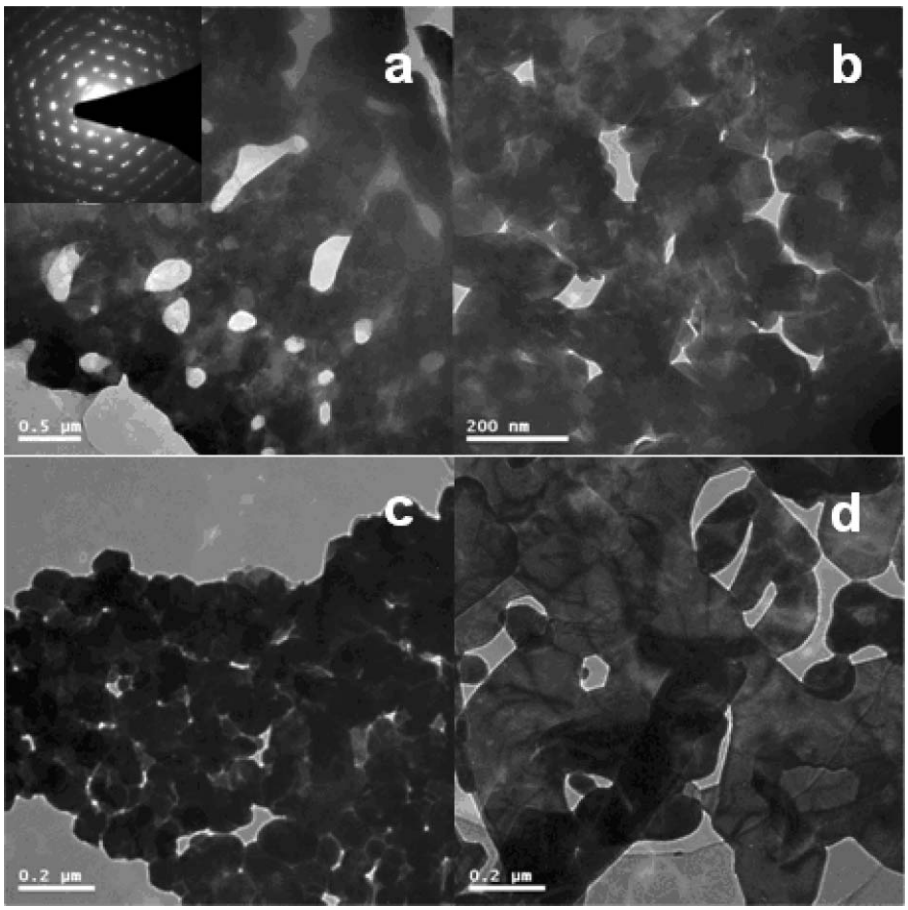

Fig. 14 TEM images of the pore wall of (a) La_2O_3 porous–macroporous materials, (b) Pr_6O_{11} porous–macroporous materials, (c, d) Nd_2O_3 porous–macroporous materials. The inset picture in (a) is the SAED pattern which indicates the single crystalline property of the La_2O_3 microflakes.

TEM images (Fig. S7) of lanthanide oxide nanofibers showed a porous structure after calcination. When using asparagines as the additive, La_2O_3, Pr_6O_{11} and Nd_2O_3 foams with porous walls were obtained (Fig. 13). From the SEM and TEM images (Fig. 14), it is observed that the macroporous walls of all these lanthanide oxides were composed of nanoflakes and microflakes, and the aggregation of nanoflakes on the microflakes gave rise to the porous structure of the lanthanide oxides.

Conclusion

Porous lanthanide oxides were fabricated by thermolysis of precursors, which were synthesized hydrothermally with lanthanide (La, Ce, Pr and Nd) salts and sodium oxalate in the presence of glutamine or asparagine, respectively. Though the chemical structures of asparagine and glutamine are similar, they exhibited greatly different complexation abilities with lanthanide cations under hydrothermal conditions. Compared to the electrostatic interaction between oxalate anions and lanthanide cations, the complexation interaction between glutamine and lanthanide cations was weaker. Using glutamine as additive, nanofibers of the crystalline oxalate precursor was produced. In contrast, the complexation ability of the asparagine with lanthanide cations was much stronger and an amorphous compound precursor with a 3D macroporous structure was fabricated. Based on the competitive complexation with lanthanide cations between oxalate anions and asparagine, variations of oxalate anions concentration and pH values of the reaction solution could tune the morphology of precursors. After calcination, porous lanthanide oxides were obtained which retained the morphologies of their corresponding precursors. Our work suggests that the complexing ability of organic molecules with metal cations could be a crucial factor for morphological control of metal salt precursors. Considering the diversity of organic additives and metal salts, it is expected that other metal oxides with complex composition and morphology could be fabricated by this organic molecule-modified precursor method.

Acknowledgements

This work was supported by NSFC (Grant Nos. 20873070 and 20973095), the National Basic Research Program of China (2009CB623502) and NCET of the Ministry of Education (NCET-07-0448).

References

1 M. E. Davis, *Nature*, 2002, **417**, 813.
2 D. M. Lyons, K. M. Ryan and M. A. Morris, *J. Mater. Chem.*, 2002, **12**, 1207.

3 Y. S. Hu, Y. G. Guo, W. Sigle, S. Hore, P. Balaya and J. Maier, *Nat. Mater.*, 2006, **5**, 713.
4 A. S. Aricò, P. Bruce, B. Scrosati, J. M. Tarascon and W. Van Schalkwijk, *Nat. Mater.*, 2005, **4**, 366.
5 Z. Tebby, O. Babot, T. Toupance, D. H. Park, G. Campet and M. H. Delville, *Chem. Mater.*, 2008, **20**, 7260.
6 C. Cannas, A. Ardu, A. Musinu, D. Peddis and G. Piccaluga, *Chem. Mater.*, 2008, **20**, 6364.
7 R. Zhu, C. Y. Jiang, B. Liu and S. Ramakrishna, *Adv. Mater.*, 2009, **21**, 994.
8 T. Sun, S. Donthu, M. Sprung, K. D'Aquila, Z. Jiang, A. Srivastava, J. Wang and V. Dravid, *Thin Solid Films*, 2009, **57**, 1095.
9 S. Li, Z. W. Li, Y. Y. Tay, J. Armellin and W. Gao, *Cryst. Growth Des.*, 2008, **8**, 1623.
10 T. Z. Ren, Z. Y. Yuan and B. L. Su, *Chem. Phys. Lett.*, 2004, **388**, 46.
11 D. M. Antonelli and J. Y. Ying, *Angew. Chem., Int. Ed. Engl.*, 1996, **35**, 426.
12 D. M. Antonelli and J. Y. Ying, *Chem. Mater.*, 1996, **8**, 874.
13 P. D. Yang, D. Y. Zhao, D. I. Margolese, B. F. Chmelka and G. D. Stucky, *Chem. Mater.*, 1999, **11**, 2813.
14 B. H. Jones and T. P. Lodge, *J. Am. Chem. Soc.*, 2009, **131**, 1676.
15 J. Sarkar, V. T. John, J. B. He, C. Brooks, D. Gandhi, A. Nunes, G. Ramanath and A. Bose, *Chem. Mater.*, 2008, **20**, 5301.
16 T. Katou, B. Lee, D. L. Lu, J. N. Kondo, M. Hara and K. Domen, *Angew. Chem., Int. Ed.*, 2003, **42**, 2382.
17 B. Z. Tian, X. Y. Liu, L. A. Solovyov, Z. Liu, H. F. Yang, Z. D. Zhang, S. H. Xie, F. Q. Zhang, B. Tu, C. Z. Yu, O. Terasaki and D. Y. Zhao, *J. Am. Chem. Soc.*, 2004, **126**, 865.
18 B. T. Holland, C. F. Blanford, T. Do and A. Stein, *Chem. Mater.*, 1999, **11**, 795.
19 X. Y. Lai, X. T. Li, W. C. Geng, J. C. Tu, J. X. Li and S. L. Qiu, *Angew. Chem., Int. Ed.*, 2007, **46**, 738.
20 D. Louër, J. P. Auffredic, J. I. Langford, D. Ciosmak and J. C. Niepce, *J. Appl. Crystallogr.*, 1983, **16**, 183.
21 V. K. Sankaranarayanan and N. S. Gajbhiye, *Thermochim. Acta*, 1989, **153**, 337.
22 V. K. Sankaranarayanan and N. S. Gajbhiye, *J. Am. Ceram. Soc.*, 1990, **73**, 1301.
23 J. I. Langford, A. Boultif, J. P. Auffredic and D. Louer, *J. Appl. Crystallogr.*, 1993, **26**, 22.
24 N. Guillou, J. P. Auffredic and D. Louer, *Powder Diffr.*, 1995, **10**, 236.
25 G. Fierro, S. Morpurgo, M. Lo Jacono, M. Inversi and I. Pettiti, *Appl. Catal., A*, 1998, **166**, 407.
26 E. Traversa, P. Nunziante, M. Sakamoto, Y. Sadaoka, M. C. Carotta and G. Martinelli, *J. Mater. Res.*, 1998, **13**, 1335.
27 M. Veith, *J. Sol-Gel Sci. Technol.*, 2008, **46**, 291.
28 M. Veith, *J. Chem. Soc., Dalton Trans.*, 2002, 2405.
29 M. Veith, M. Haas and V. Huch, *Chem. Mater.*, 2005, **17**, 95.
30 E. V. Tsipis, V. V. Kharton, I. A. Bashmakov, E. N. Naumovich and J. R. Frade, *J. Solid State Electrochem.*, 2004, **8**, 674.
31 G. J. Zhang, Z. R. Shen, M. Liu, C. H. Guo, P. C. Sun, Z. Y. Yuan, B. H. Li, D. T. Ding and T. H. Chen, *J. Phys. Chem. B*, 2006, **110**, 25782.
32 C. C. Yu, L. X. Zhang, J. L. Shi, J. J. Zhao, J. H. Gao and D. S. Yan, *Adv. Funct. Mater.*, 2008, **18**, 1544.
33 M. Liu, G. J. Zhang, Z. R. Shen, P. C. Sun, D. T. Ding and T. H. Chen, *Solid State Sci.*, 2009, **11**, 118.
34 S. L. Zhong, J. S. Hu, L. J. Wan and W. G. Song, *Chem. Commun.*, 2008, 1184.
35 C. L. Gao, W. L. Zhang, H. B. Li, L. M. Lang and Z. Xu, *Cryst. Growth Des.*, 2008, **8**, 3785.
36 H. P. Zhou, Y. W. Zhang, R. Si, L. S. Zhang, W. G. Song and C. H. Yan, *J. Phys. Chem. C*, 2008, **112**, 20366.
37 H. D. Yu, D. S. Wang and M. Y. Han, *J. Am. Chem. Soc.*, 2007, **129**, 2333.
38 M. Y. Li, W. S. Dong, C. L. Liu, Z. T. Liu and F. Q. Lin, *J. Cryst. Growth*, 2008, **310**, 4628.
39 Z. A. Zang, H. B. Yao, Y. X. Zhou, W. T. Yao and S. H. Yu, *Chem. Mater.*, 2008, **20**, 4749.
40 J. Y. Liu, Z. Guo, F. L. Meng, T. Luo, M. Q. Li and J. H. Liu, *Nanotechnology*, 2009, **20**, 125501.
41 Z. R. Shen, G. J. Zhang, H. J. Zhou, P. C. Sun, B. H. Li, D. T. Ding and T. H. Chen, *Adv. Mater.*, 2008, **20**, 984.
42 Z. R. Shen, J. G. Wang, P. C. Sun, D. T. Ding and T. H. Chen, *Chem. Commun.*, 2009, 1742.
43 H. Tong, W. T. Ma, L. L. Wang, P. Wan, J. M. Hu and L. X. Cao, *Biomaterials*, 2004, **25**, 3923.
44 P. Cheng and D. K. Bohme, *J. Phys. Chem. B*, 2007, **111**, 11075.
45 M. Oh and C. A. Mirkin, *Nature*, 2005, **438**, 651.
46 G. A. Santillan and C. J. Carrano, *Cryst. Growth Des.*, 2009, **9**, 1590.
47 T. J. Burchell, D. J. Eisler, M. C. Jennings and R. J. Puddephatt, *Chem. Commun.*, 2003, 2228.
48 J. A. Rood, W. C. Boggess, B. C. Noll and K. W. Henderson, *J. Am. Chem. Soc.*, 2007, **129**, 13675.
49 S. F. Shao, G. J. Zhang, H. J. Zhou, P. C. Sun, Z. Y. Yuan, B. H. Li, D. T. Ding and T. H. Chen, *Solid State Sci.*, 2007, **9**, 725.